文章编号：1006-3471(2007)01-0012-07

Charge-Discharge Behaviors and Properties of a Lab-Scale All-Vanadium Redox-Flow Single Cell

ZHAO Ping, ZHANG Hua-min*,
WEN Yue-hua, YI Bao-lian
(1. *PEMFC Key Materials & Technology Lab.*, *Dalian Institute of Chemical Physics*, *Chinese Academy of Sciences*, *Dalian*, *Liaoning*, 116023, *China*)

Abstract: An experimental setup with two external saturated calomel reference electrodes (SCE) and two flow cells was established for flow battery research application. By using this setup, the cell voltage, potentials and open circuit potentials of the positive and negative electrodes for a lab-scale flow battery single cell, could be determined simultaneously during charge-discharge (C-D) cycle test. Then, the ohmic internal resistance drop (*iR* drop), overpotentials at the negative and positive electrodes of the cell during C-D process, were calculated. The average *iR* drop accounts for about 74% of the total voltage losses during the C-D cycle at current density of 60 mA · cm^{-2}, suggesting the voltage efficiency (VE) of vanadium redox-flow battery (VRB) single cell with graphite felt as electrodes and Nafion 117 as battery separator, was limited by the cell ohmic internal resistance. The C-D curves show that the appearance of the end-point of discharge is mainly due to the zoom of negative electrode over potential. The VRB single cell designed in this work achieves an excellent performance, with voltage and energy efficiency up to ca. 89% and 85%, respectively, at C-D current density of 60 mA · cm^{-2}, indicating structure of the cell is reasonable, and graphite felt is suitable for VRB electrode application.

Key words: all-vanadium redox-flow cell; graphite felt; electrode polarization; ohmic internal resistance
CLC Number: O 646; TM 911 **Document code**: A

1 Introduction

The vanadium redox-flow battery (VRB) proposed by Skyllas-kazacos and co-workers[1-2] has received considerable attention all over the world[3-16], and been considered a promising energy storage technology for stationary applications, due to its long cycle life, flexible design and deep-discharge capability[3-8].

The performance of a redox-flow cell may be evaluated, from the engineering point of view, by its coulombic, voltage and energy efficiencies [9] (hereafter abbreviated as CE, VE and EE, respectively). In fact, CE, VE and EE of the cell are not independent, and EE can be defined as the product of VE and CE [9]. The EE of a cell should be governed by various factors [13], including: (i) resistive losses in the electrolytes, membrane and electrodes (i. e. *iR* drop), (ii) mass transfer losses in the electrolyte (i. e. concentration polarization), (iii) loss of voltage due to large overpotential (i. e. activation polarization) for electrode reactions with slow kinetics, (iv)

Received date: 2006-03-10, accepted date: 2006-05-20 * Corresponding Author, Tel: (86-411)84379072, E-mail: zhanghm@dicp.ac.cn
Supported by Hi-Tech Research and Development Program of China (2005AA516020)

loss of faradic efficiency due to possible side reactions, and (v) loss of faradic efficiency due to crossover of ions through the membrane. The above factors affecting the EE of the cell may be divided into two categories. One can be called as VE factors, i. e., the factors (i) to (iii), which control the voltage losses of the cell during charge-discharge (C-D) cycle, and the other is CE factors, including the factors (iv) and (v). The factors governing CE (i. e. the CE factors) are related closely with the membrane type (factor (v)) and the redox couple (factor (iv)) used in the flow cell. Leaving the CE aside, to realize high EE of a flow cell, the VE factors (i) to (iii) should be as low as possible. Therefore, if the extent of the effect of each VE factor on cell VE during C-D cycle can be identified, the flow cell performance could be improved more efficiently and intentionally.

In the present work, the cell voltage, potentials and open circuit potentials of the positive and negative electrodes of a lab-scale VRB single cell were simultaneously determined during C-D cycle tests. The *iR* drop of the cell and the overpotentials of the positive and negative electrodes during charge and discharge processes were then calculated. The relative extent of the effect of each VE factor on cell VE was, thus, disclosed during C-D cycle. Also, other properties corresponding to C-D process of the cell were studied and discussed.

2 Experimental

2.1 Electrode Material and Electrolyte

Samples of 3 mm thick polyacrylonitrile (PAN)-based graphite felt (GF) were chosen as both the positive and negative electrode materials. As shown in Fig. 1, the GF is composed of graphite fibers with an average diameter of about 17 μm, and possesses a typical 3D structure. Some properties of the as-received GF were summarized in Table 1.

Vanadyl sulfate was purchased from Shanghai Fine Chemicals Factory. 1.5 mol/L $VOSO_4$ in 3 mol/L H_2SO_4 solution (i. e. V(IV) electrolyte) was prepared using blue $VOSO_4$ salt, analytical grade H_2SO_4 and deioned water. V(III) electrolyte was prepared by the electrochemical reduction of the above V(IV) solution [14].

Tab. 1　Properties of the as-received graphite felt used in this study

Bulk density / g · cm^{-3}	Porosity / %	Electrical resistance /Ω · cm	Carbon content / %
0.15	91.3	0.04	90 ~ 95

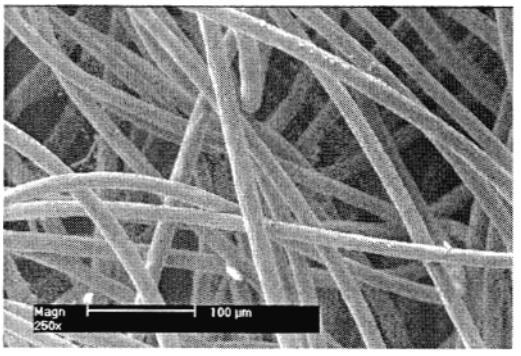

Fig. 1　SEM image of the as-received graphite felt (250 ×)

2.2 Experimental Setup and Charge-discharge Tests

The flow cell constructed for this study is the same as that used in Ref. [17]. The experimental setup, as shown in Fig. 2, is a modified version of that in literature [17]. The experimental apparatus was composed of two flow cells (cell 8 and 9) both with an effective electrode area of 20 mm × 25 mm. The only difference between these two cells lies in the separator used, namely, Nafion® 117 for cell 8 and 1.8 mm thick PVC plate for cell 9. During the experiments, the anolyte (negative electrolyte) and catholyte (positive electrolyte) were pumped first through cell 9, then via cell 8, and finally flowed back into their own reservoir. Four digital voltmeters were used to measure the electrode potentials between cell electrodes and saturated calomel reference electrodes (SCE) during test. In order to record the 4 potentials at the same time, a video camera (QuickCam® Pro 4000, Logitech) was employed. The open circuit positive and negative electrode potentials were deter-

mined at cell 9. An Arbin battery test instrument (BT2000, Arbin Instrument Corp., USA) was used to charge and discharge the cell 8.

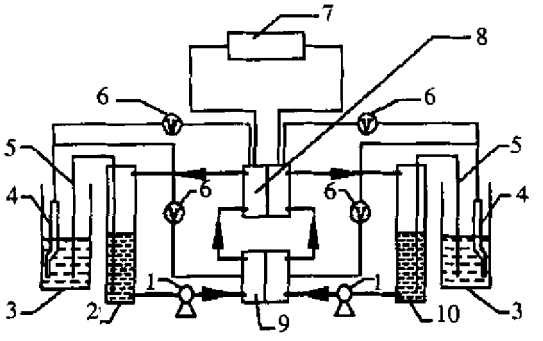

Fig. 2 Schematic diagram of the experimental setup for flow battery research
1) pump, 2) anolyte tank, 3) saturated KCl solution, 4) SCE, 5) saturated KCl salt bridge, 6) digital voltmeter, 7) Arbin instrument, 8, 9) flow cell, 10) catholyte tank

At the beginning of charge/discharge cycles, 30 mL 1.5 mol/L V(III) in 3 mol/L H_2SO_4 solution and 30 mL 1.5 mol/L V(IV) in 3 mol/L H_2SO_4 solution were used as the anolyte and catholyte, respectively. The electrolytes were kept at 26 ± 0.5 ℃ by using a thermostated water bath. The flow rates of the two electrolytes were both about 30 mL/min. The C-D experiment was controlled automatically by Arbin between set upper (1.7 V) and lower (0.9 V) voltage limits and proceeded at a constant current density of 40, 60, 80, 100 mA · cm^{-2}, respectively. The C-D reactions on electrodes would be[14]:

$$\text{Positive electrode: } VO^{2+} + H_2O \underset{\text{discharge}}{\overset{\text{charge}}{\rightleftharpoons}} VO_2^{+} + 2H^{+} + e \quad (1)$$

$$\text{Negative electrode: } V^{3+} + e \underset{\text{discharge}}{\overset{\text{charge}}{\rightleftharpoons}} V^{2+} \quad (2)$$

The electrical balance was achieved mainly by the transport of H^+ in the electrolytes across the membrane during operation of the cell.

3 Results and Discussion

Typical charge-discharge curves for the VRB single cell at the current density of 60 and 80 mA · cm^{-2} are depicted in Fig. 3. The cell positive and negative electrode potentials (vs. SCE) during charge and discharge are also illustrated. Apart from the difference in charge and discharge time, as shown in Fig. 3, the trends of the curves obtained at different current densities are almost the same. It can also be seen from Fig. 3 that the cell voltage changes smoothly with time, except for the end period of charge and discharge. An apparent turning point occurs at the cell discharge curve of about 1.1 V, then the discharge voltage drops swiftly and soon reaches the end potential of 0.9 V. It is clear, from Fig. 3, that the diving of the cell voltage can mainly be attributed to the zoom of the negative potential at the end of discharge.

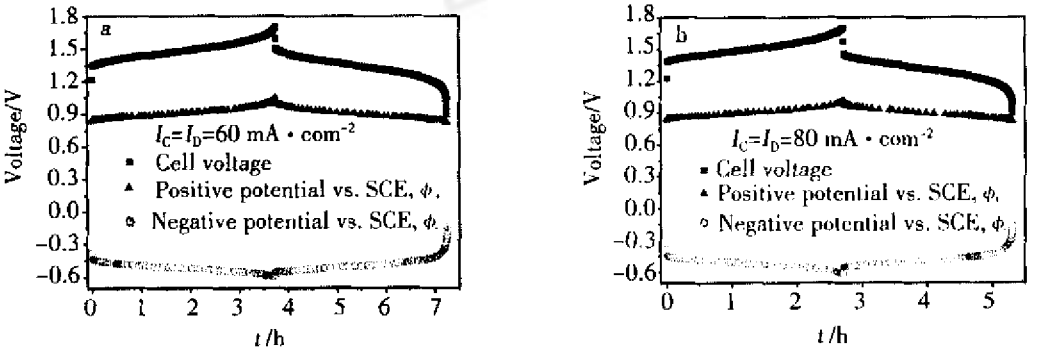

Fig. 3 Charge-discharge curves for VRB single flow cell employing graphite felt as electrode materials
anolyte: 30 mL 1.5 mol/L V(III) in 3 mol/L H_2SO_4 aq. solution, catholyte: 30 mL 1.5 mol/L V(IV) in 3 mol/L H_2SO_4 aq. solution, flow rate of both electrolytes: 30 mL/ min, temperature: 26 ℃, cell voltage upper limit = 1.7 V, lower limit = 0.9 V, geometric electrode area = 5 cm^2, Nafion® 117 membrane

The total cell voltage for charging and discharging is given, respectively, by

$$V_C = \varphi_+ - \varphi_- + iR = (\varphi_{+,OC} + \Delta\varphi_+) - (\varphi_{-,OC} + \Delta\varphi_-) + iR \quad (3)$$

and

$$V_D = \varphi_+ - \varphi_- - iR = (\varphi_{+,OC} + \Delta\varphi_+) - (\varphi_{-,OC} + \Delta\varphi_-) - iR \quad (4)$$

Where φ_+ and φ_- are the positive and negative electrode potential during charging or discharging, respectively; $\varphi_{+,OC}$ and $\varphi_{-,OC}$, the open circuit potentials at positive and negative electrodes; $\Delta\varphi_+$ and $\Delta\varphi_-$, the overpotentials at the positive and negative electrodes ($\Delta\varphi = \varphi - \varphi_{OC}$); i, the charge or discharge current; and R, the ohmic internal resistance of cell.

The sharp rise of φ_- (see Fig. 3) at the end of the discharge caused evidently a rapid fall of the V_D according to Eq. 4. The zoom of φ_- at the end of discharge was mainly caused by the dramatic increase of the negative electrode overpotential $\Delta\varphi_-$, as shown in Fig. 4. This zoom of φ_- could be attributed to severe concentration polarization due to the insufficiency of V^{2+} in the anolyte at the end of the discharge. In this study, a piece of Nafion® 117 membrane was used as the separator. The V^{2+} and V^{3+} ions in the anolyte could permeate through Nafion® 117 membrane more easily than the VO^{2+} and VO_2^+ in the catholyte[15], resulting in the imbalance of the amount of V^{2+} and VO_2^+, hence the relatively high concentration polarization of the negative electrode reaction at the end of discharge process can be expected.

Based on the data of Fig. 3, the iR drop of the cell during charge and discharge processes can be calculated, by Eqs. (3) and (4), so that the cell ohmic internal resistance R was obtained, as illustrated in Fig. 5. It is clear from Fig. 5, the ohmic internal resistance for the discharge process is a little higher than that for the charge.

The average values of cell voltage, overpotentials of positive and negative electrodes, and internal resistance (R) of the cell during C-D processes are calculated by integration method from Figs. 3, 4 and 5, respectively, and summarized in Table 2. As can be

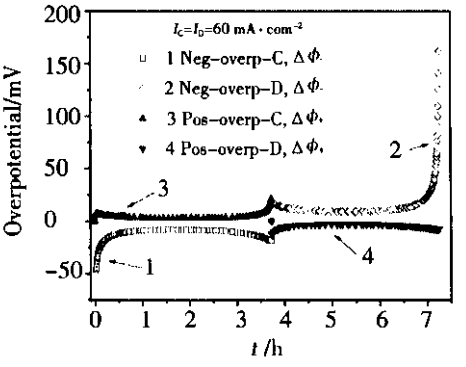

Fig. 4　Variation of the overpotentials of negative and positive electrodes during charge-discharge cycle at current density of 60 mA · cm^{-2}
other experimental conditions as in Fig. 3
legend notes, C: means charge, D: discharge, Neg: negative electrode, Pos: positive electrode, overp: overpotential

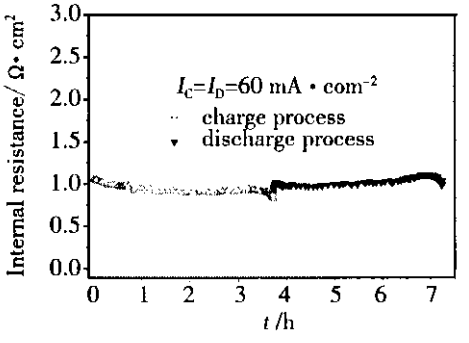

Fig. 5　Variation of ohmic internal resistance of the VRB single cell during charge-discharge cycle at current density of 60 mA · cm^{-2}
other experimental conditions as in Fig. 3

seen from Table 2, the average ohmic internal resistance for charge process is a little lower than that for discharge. This could mainly be attributed to: (1) effect of the direction of electric field (EF) generated by cell voltage on the transport rate of charge-carrying H^+ in the electrolyte through cell separator, and hence on the ohmic internal resistance of the flow cell during charge/discharge cycle. For charging process, the direction of EF is the same as that of movement of H^+, whereas, the directions of EF and the transport of H^+ are just opposite during discharging. (2) effect of variation of the H^+ concentration in the electrolyte

Tab. 2 The average values of iR, overpotentials at the positive electrode and negative electrode, cell voltage, and ohmic internal resistance of the VRB single cell during charge-discharge cycles at different current densities. Experimental conditions as in Fig. 3

Current density / mA · cm^{-2}	*iR* / mV		Positive overpotential/ mV		Negative overpotential/ mV		Cell voltage/V		Ohmic internal resistance/Ω · cm^2	
	charge	discharge	charge	discharge	charge	discharge	charge	discharge	charge	discharge
40	37.95	38.11	4.94	−4.99	−7.50	9.63	1.46	1.36	0.95	0.95
60	55.65	61.03	6.18	−6.29	−13.08	16.13	1.49	1.33	0.93	1.02
80	77.75	83.18	6.70	−6.93	−19.20	22.53	1.51	1.30	0.97	1.04
100	97.15	104.10	7.52	−7.84	−25.54	29.32	1.53	1.26	0.97	1.04

on the cell ohmic resistance during charge/discharge cycle. The H^+ concentration increases during the charge and decreases during the discharge of the flow cell (by Eq. (1)). Increasing the concentration of H^+ in the solution will decrease the resistance of ion exchange membrane[11] and the electrolyte[12], accordingly, the ohmic internal resistance of the cell will change during charge/discharge cycle.

The average positive overpotentials for both of the charge and discharge processes are less than the negative ones, as shown in Table 2, indicating the graphite felt electrode has higher electrocatalytic activity for the positive redox couple of VRB single cell. In other words, the electrode reaction kinetics for VO^{2+}/VO_2^+ is somewhat faster than that for V^{2+}/V^{3+} on a graphite electrode, which is consistent with the results obtained on carbon-based electrodes [8,13].

Fig. 6 compares the absolute average values of the *iR*, as well as the positive and negative electrode overpotentials (data from Table 2) of a charge/discharge cycle at the current density of 60 mA cm^{-2}. As shown in Fig. 6, relatively high *iR* drop dominates the overall voltage losses, by contrast, the subtotal of the overpotentials at negative and positive electrodes only contribute ca. 26% to the total voltage losses during the C-D cycle. This result implies that, to realize performance of higher VE of the VRB single cell, we should strive to reduce the resistive losses in the electrolytes, membrane and electrodes of the cell. Of course, enhancing of the electrocatalytic activity of the electrode materials for the VRB redox couples can also be favorable for the improvement of VE of the cell. However, the effect can be anticipated to be relatively minor.

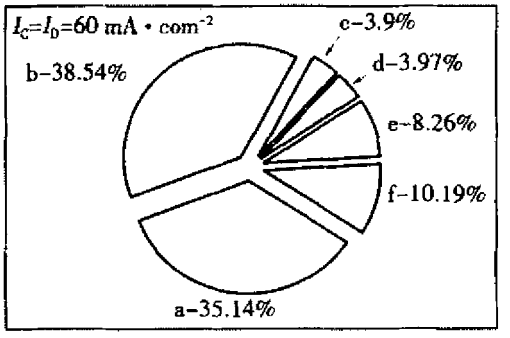

Fig. 6 Comparison of the absolute average values of iR, positive and negative electrode overpotentials during a charge-discharge cycle at current density of 60 mA · cm^{-2}
a: iR-C, b: iR-D, c: Pos-overp-C, d: Pos-overp-D, e: Neg-overp-C, f: Neg-overp-D
Experimental conditions as in Fig. 3, legend notes as in Fig. 4

Fig. 7 shows the variation of the cell efficiencies and power density with the current density for the VRB single cell used in this study. The power density in Fig. 7 is the product of the discharge current density and the corresponding discharge cell voltage listed in Table 2. Increasing the current density is seen to decrease the cell VE as expected, due to increased *iR* drop and polarization losses of negative and positive electrodes, as shown in Table 2. At higher current densities the CE increases, however, because of the lower self-discharge across the membrane in the shorter cycle time (see Fig. 3). The VE, EE and power density of the cell at a constant C-D current density of 60 mA · cm^{-2} were about 89.3%, 84.8%, and 79.8 mWcm^{-2}, respectively, as presented in Fig. 7,

and these results were much better than that obtained by Sun[16]. With an obtained VE of 89.3%, the total lost efficiency caused by overpotentials and *iR* drop can be calculated to be 10.7%. Based on the results listed in Fig. 6, we know that the lost efficiency caused by the total overpotentials at the negative and positive electrode during charge and discharge processes is only 2.8%, and the rest 7.9% can be ascribed to the *iR* drop. Such low loss in VE indicates that the graphite felt is the suitable electrode material with high electrochemical activity for VRB and the structure of the cell used in this work is reasonable.

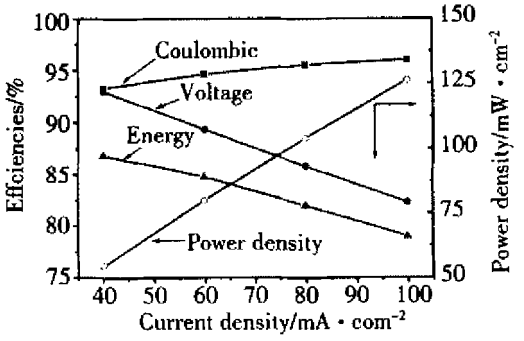

Fig. 7　Effect of current density on the efficiencies and power density of VRB single cell
experimental conditions as in Fig. 3

4　Conclusions

1) The rapid increase of negative electrode potential, caused by severe concentration polarization, due to the exhausting of V^{2+} in the anolyte at the end of discharge, is the main factor which resulted in the lower limit of the cell discharge voltage for VRB single cell.

2) The relatively high *iR* drop governed the voltage efficiency, and hence the overall energy efficiency of the VRB single cell. By contrast, the positive and negative electrode overpotentials contributed to a less extent to the total overvoltage during the charge-discharge cycle.

3) The internal ohmic resistance of VRB single cell for the charge process is a little lower than that for the discharge, which could be attributed to the effect of the direction of electric field generated by cell voltage on the charge-carrying H^+ transport rate across the cell separator, and the effect of variation of the H^+ concentration on the flow cell resistance during charge-discharge cycle.

4) Graphite felt possess sufficient electrocatalytic activity to the negative and positive redox reactions of VRB, and is a kind of suitable electrode material.

References:

[1] Sum E, Rychcik M, Skyllas-Kazacos M. Investigation of the V(V)/V(IV) system for use in the positive half-cell of a redox battery[J]. J Power Sources, 1985,16(2):85~95.

[2] Sum E, Skyllas-Kazacos M. A study of the V(II)/V(III) redox copule for redox flow cell applications[J]. J Power Sources, 1985,15(2-3):179~190.

[3] CUI Yan-hua (崔艳华), MENG Fan-ming (孟凡明). Development and prospect of vanadium energy storage system[J]. Chinese Journal of Power Sources (in Chinese), 2005, 29(11):776-780.

[4] LIU Su-qin (刘素琴), HUANG Ke-long (黄可龙), LIU You-nian (刘又年), et al. The development and research progress in an energy storage unit-the vanadium redox flow battery[J]. Battery Bimonthly (in Chinese), 2005, 35(5):356-359.

[5] DONG Quan-feng (董全峰), ZHANG Hua-min (张华民), JIN Ming-gang (金明钢), et al. Research progresses in a flow redox battery[J]. Electrochemistry(in Chinese), 2005, 11(3):237-243.

[6] Luo X, Lu Z, Xi J, et al. Influences of permeation of vanadium ions through PVDF-g-PSSA membranes on performances of vanadium redox flow batteries [J]. J Phys Chem B,2005,109(43):20310-20314.

[7] Gattrell M, Qian J, Stewart C, et al. The electrochemical reduction of VO_2^+ in acidic solution at high overpotentials [J]. Electrochim Acta, 2005, 51(3):395-407.

[8] Fabjan Ch, Garche J, Harrer B, et al. The vanadium redox-battery:an efficient storage unit for photovoltaic systems [J]. Electrochim Acta,2001,47(5):825-831.

[9] Sukkar T, Skyllas-Kazacos M. Membrane stability studies for vanadium redox cell applications [J]. J Appl Electrochem,2004, 34(2):137-145.

[10] Tian B, Yan C W, Wang F H. Modification and evaluation of membranes for vanadium redox battery appli-

cations [J]. J Appl Electrochem, 2004, 34 (12): 1205-1210.

[11] TAN Ning (谭宁), HUANG Ke-long (黄可龙), LIU Su-qin (刘素琴), Studies on ion exchange membrane performance in vanadium solution for all vanadium flow battery [J]. Chinese Journal of Power Sources (in Chinese), 2004, 28 (12): 775-778, 802.

[12] Kazacos M, Cheng M, Skyllas-Kazacos M. Vanadium redox cell electrolyte optimization studies [J]. J Appl Electrochem, 1990, 20(3): 463-467.

[13] Yamamura T, Watanabe N, Yano T, et al. Electron-transfer kinetics of Np^{3+}/Np^{4+}, NpO_2^{+}/NpO_2^{2+}, V^{2+}/V^{3+}, and VO^{2+}/VO_2^{+} at carbon electrodes [J]. J Electrochem Soc 2005, 152 (4): A830-A836.

[14] Rychcik M, Skyllas-Kazacos M. Evaluation of electrode materials for vanadium redox cell [J]. J Power Sources, 1987, 19 (1): 45-54.

[15] Mohammadi T, Chieng S C, Skyllas-Kazacos M. Water transport study across commercial ion exchange membranes in the vanadium redox flow battery [J]. J Membr Sci, 1997, 133(2): 151-159.

[16] Sun B, Skyllas-Kazacos M. Modification of graphite electrode materials for vanadium redox flow battery application-I. Thermal treatment [J]. Electrochim Acta, 1992, 37(7): 1253-1260.

[17] Zhao P, Zhang H, Zhou H, et al. Nickel foam and carbon felt applications for sodium polysulfide/bromine redox flow battery electrodes [J]. Electrochim Acta, 2005, 51 (6): 1091-1098.

全钒液流单电池充放电行为及特性研究

赵 平, 张华民*, 文越华, 衣宝廉

(中国科学院大连化学物理研究所 质子交换膜燃料电池关键材料与技术组, 辽宁 大连 116023)

摘要: 建立具有外置双饱和甘汞参比电极及双液流电池的实验装置系统. 使用该装置可在同一时刻同时测定小型液流单电池充放电时的电池电压、电池正负极电位及正负极开路电位, 进而计算充放电过程电池的欧姆内阻降(*iR*)及其正负极过电位. 以石墨毡为电极、Nafion 117 作隔膜的全钒液流单电池, 在 60 mA · cm^{-2} 电流密度下, 每一充放电循环的平均 *iR* 降约占总电压损耗的 74%, 表明该电池的电压效率受制于电池的欧姆内阻. 充放电曲线显示, 电池放电终点之所以出现主要是由于电池负极电位在放电末期的快速上升而引起的. 本文设计的全钒单电池于 60 mA · cm^{-2} 下工作时, 其电压及能量效率分别达 89% 和 85%, 表明该电池结构合理, 且石墨毡是钒电池合适的电极材料.

关键词: 全钒液流电池; 石墨毡; 电极极化; 欧姆内阻